Preparation and Analysis of Lead Copper Sulfide Thin Film Heterojunctions Using Vacuum Thermal Deposition

Sura N. Taraad [1]
Mustafa A. Abbas [2]

[1] Diwaniyah Education Directorate, Ministry of Education, Diwaniyah, IRAQ
[2] Department of Physics, College of Education, University of Al-Qadisiyah, Al-Qadisiyah, IRAQ

This study investigates the structural, optical, and electrical properties of PbS/CuS composite thin films prepared via vacuum thermal evaporation on (111)-oriented single-crystal Si substrates of both p-type and n-type. XRD revealed a polycrystalline cubic structure with increased crystallite size. AFM confirmed uniform surface distribution, while FESEM showed nanostructured morphology. Optical absorbance decreased with higher additive ratios, suggesting a transition toward an amorphous-like structure. Hall effect measurements indicated p-type conductivity dominated by holes. I-V and C-V analyses were performed for the P-(PbS/CuS)/P-Si and P-(PbS/CuS)/N-Si heterojunctions.

***Keywords*:** PbCuS; Composite films; Electrical resistivity; Depletion region
Received: 19 February 2025; **Revised:** 8 April 2025; **Accepted:** 15 April 2025

1. Introduction

Semiconductors are materials in which the flow of electric current is relatively difficult compared to conductors, and their electrical conductivity can be enhanced by introducing other elements in trace amounts. The electrical resistance of semiconductors lies between that of conductors and insulators. Semiconductors are the foundation of modern technology, including radios, computers, telephones, televisions, and various electronic components such as solar cells, transistors, light-emitting diodes (LEDs), and diodes. Solar panels are a prime example of semiconductor materials as they convert light energy into electrical energy, where electrons carry the current. In semiconductors, electrical current is conducted through a flow of electrons toward the positive electrode and a flow of holes toward the negative electrode [1-3].

Among the essential elements for semiconductors, silicon is the most preferred for manufacturing most commercial devices. This is because silicon conducts electricity at specific temperatures, whereas germanium conducts at all temperatures. Silicon is also abundant and cost-effective. Pure semiconductors are referred to as "intrinsic semiconductors," and their conductivity can be enhanced by adding impurities, a process known as doping. This involves melting the material, introducing impurities, and allowing it to cool to form a new crystal structure different from the original [4,5].

Copper sulfide (CuS) belongs to an important class of semiconducting compounds known as chalcogenides, which consist of a metal combined with a Group VI element such as sulfur or selenium. These materials have garnered significant attention due to their diverse properties and high potential for tailoring their characteristics. CuS exists in five stable phases at room temperature, ranging from copper-rich phases such as Covellite (CuS) to other forms like chalcocite (Cu_2S), Djurleite, and Anillite [6,7].

Covellite (CuS), on the other hand, crystallizes in a hexagonal system and is commonly found as thin layers or granular aggregates in association with other copper minerals. It has a density of 4.6–4.76 g/cm^3, exhibits a metallic luster, and has a blue-violet color. Although Covellite is less common, it is often found in the same locations as chalcocite, but it is not considered a major source of copper [8].

Lead sulfide (PbS) is a well-known semiconducting compound with excellent photoconductive properties in the infrared range (800–3000 nm). It is widely used in the production of Photodetectors for both military and civilian applications. PbS is a polar semiconductor belonging to Group IV-VI compounds and has a face-centered cubic (FCC) crystal structure [9-11].

PbS exhibits a mixed chemical bonding nature, with ionic-covalent bonds where the ionic bonding dominates over the covalent bonding. This unique bonding structure makes PbS similar to other ionic compounds. In 1956, Krebs [12] proposed a bonding model for PbS, describing the presence of ionic-covalent bonds. In this structure, sulfur ions possess a single electron pair in the S-state and three electron pairs in the P-state, while lead ions have three vacant levels in the P-state. Each sulfur ion is octahedral coordinated with six lead ions, and similarly, each lead ion is surrounded by six sulfur ions. This bonding arrangement results in a highly stable and ordered structure [13].

Heterojunctions are among the most important technologies due to their applications in various fields,

including high-efficiency solar cells. A heterojunction can be defined as a semiconductor diode formed by an intimate contact between two materials differing in dielectric constant, optical bandgap, work function, and electron affinity [14,15].

Heterojunctions are classified based on the transition distance between the two materials into abrupt heterojunctions and graded heterojunctions. If both materials have the same conductivity type, the heterojunction is termed isotype heterojunction (e.g., p–p or n–n). Conversely, if the conductivity types are different, it is called an anisotype heterojunction (e.g., p–n or n–p) [16].

Different semiconductor materials generally do not share the same bandgap, which creates a discontinuity in the energy bands at the interface. This leads to non-uniformity in the electronic structure. Consequently, the current–voltage (I–V) characteristics of heterojunctions differ from those of homojunctions, which are formed between two similar semiconductor materials [17,18].

The electrical properties of a heterojunction are among its most distinctive features. These include current–voltage (I–V) and capacitance–voltage (C–V) characteristics, which provide critical information about the band structure of the heterojunction, such as the type of junction, built-in potential, and methods of optimizing the fabricated devices. In this study, both I–V and C–V characteristics were investigated.

The study of I–V characteristics is essential to understand the mechanisms of electrical conduction. It is commonly used to determine the built-in potential of the heterojunction and the energy band discontinuity (ΔE) at the interface. I–V characteristics can be classified based on the type of bias—forward or reverse. For forward bias, the relationship of the I–V characteristics can be described by the following equation [19]:

$$J = J_{st}\left[exp\left(\frac{eV}{k_BT}\right) - 1\right] \quad (1)$$

The reverse saturation current density (J_{st})s given by the following equation:

$$J_{st} = A^*T^2 exp\left[\frac{-e(\phi_{B0}-\Delta\phi_{Bi})}{k_BT}\right] \quad (2)$$

where ϕ_{B0} represents the true potential barrier, and $\Delta\phi_{Bi}$ is the reduction in the barrier height due to the effect of the image force

$$\phi_{Bn} = \phi_{B0} - \Delta\phi_{Bi} \quad (3)$$

Under standard conditions for a diode, the current relationship is given as follows:

$$J = J_{st} exp\left(\frac{eV}{nk_BT}\right)\left[1 - exp\left(\frac{-eV}{k_BT}\right)\right] \quad (4)$$

This equation can be modified under the condition $V>3k_BT/e$ to:

$$J = J_{st} exp\left(\frac{eV}{nk_BT}\right) \quad (5)$$

Where n is the ideality factor

$$n = \frac{e}{k_BT}\left(\frac{\partial V}{\partial(lnI)}\right) \quad (6)$$

The saturation current density (J_{st}) can be obtained by extrapolating the straight line to zero voltage, allowing the barrier height to be determined using the following equation:

$$\phi_{Bn} = \frac{k_BT}{e} ln\left(\frac{A^*T^2}{J_{st}}\right) \quad (7)$$

Anderson presented a relationship to calculate the capacitance per unit area of a capacitor associated with charge transfer. This relationship is analogous to the standard equation for a parallel-plate capacitor, where the separation between the plates is represented by the width of the depletion region [20,21]:

$$C = \frac{dQ}{dV} = \frac{\varepsilon_s}{W} \quad (8)$$

where dQ is the partial change in the charge of the depletion layer per unit area due to the change in the applied voltage, ε_s is the permittivity of the semiconductor, and W is the width of the depletion region

In the case of forward bias, a significant current flows through the junction, and a large number of mobile carriers are present in the depletion region [1].

The barrier height can also be determined from the capacitance measurement of the device. By plotting the relationship between the applied voltage and the reciprocal of squared capacitance ($1/C^2$), the intercept on the voltage axis provides the barrier height using the following equation:

$$\phi_{Bn} = V_{bi} + \phi_n + \frac{k_BT}{e} - \Delta\phi \quad (9)$$

where V_{bi} is the intercept on the voltage axis, and ϕ_n is the depth of the Fermi level below the conduction band edge, which can be calculated if the doping concentration is known

In general, the Hall Effect can be defined as the deflection of current in a metallic strip due to a magnetic field. When a magnetic field (B_z) is applied to a semiconductor perpendicular to the direction of electric current, the charge carriers are deflected to one side, causing a voltage difference across the semiconductor. This voltage, known as the Hall voltage (V_H) , is accompanied by an electric field referred to as the Hall field (E_H) [1]. This is illustrated in Fig. (1).

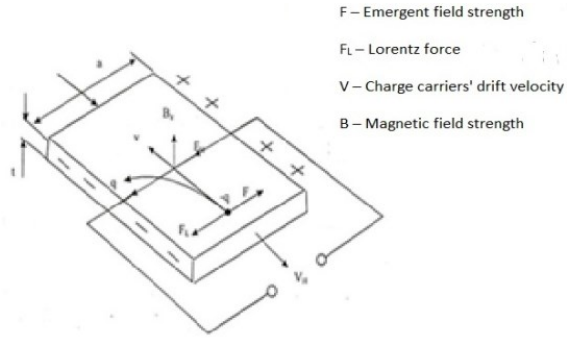

Fig. (1) Description of Hall effect diagram [1]

Hall coefficient (R_H) can be found from the relationship [1]:

$$R_H = \frac{V_H}{I} \cdot \frac{t}{B} \quad (10)$$

where I is electric current passing through the metal sheet, t is the thickness of the metal sheet, B is the magnetic field strength

The negative slope of Eq. (10) indicates that the charge carriers have a negative sign and the metal sheet contains a flow of electrons (n-type), while the positive slope indicates that the charge carriers have a positive sign and the metal sheet contains a flow of holes (p-type). The concentrations of charge carriers can be calculated using the two relationships [22]:

$$R_H = \frac{-1}{n_e} \quad (11)$$

$$R_H = \frac{1}{p_h} \quad (12)$$

where n_e is the concentration of the negative charge carriers (electrons), p_h is the concentration of the positive charge carriers (holes), and e is the electron charge

2. Methodology

A locally manufactured vacuum deposition system (thermal evaporation) was employed. The system was thoroughly cleaned from the inside using alcohol to prevent contamination of the substrates with residues from previously deposited materials. At this stage, the compound resulting from PbS+CuS was evaporated with different addition ratios of CuS (10%, 15%, and 20%). The material to be deposited was placed inside a resistive heater made of tungsten, shaped like a boat, with a melting point significantly higher than that of the material to be deposited. The boat was connected to two electrodes linked to an electrical power source within the system, which was used for heating. The substrates were positioned on a special holder, perpendicular to the boat, at a distance of 10 cm.

The electrical current applied to the electrodes was gradually increased, causing the material to begin melting. With a further gradual increase in current, the material started to glow, indicating the onset of evaporation and the deposition of the film onto the substrate. After completing the material deposition, the current was gradually reduced, and the system was left operational, maintaining the prepared samples inside the vacuum chamber under high pressure for no less than 30 minutes to prevent oxidation of the samples.

3. Results and Discussion

Figure (2) shows the X-ray diffraction (XRD) patterns for the thin PbS/CuS films prepared with different addition ratios of CuS (10%, 15%, 20%). The results revealed that all the prepared films have a polycrystalline structure and a cubic phase. For the film with 10% CuS, the predominant growth orientation is (111). In contrast, for the 15% and 20% CuS addition, the dominant growth orientation shifts to (222). It is observed that the number of peaks varies with the CuS concentration, with the highest number of peaks occurring in the film prepared with 10% CuS. Table (1) lists the inter-planer spacing, peak positions, and Miller indices for the PbS/CuS thin films prepared with different ratios.

When comparing the peak positions with the standard data (ICDD) for the individual components, it is evident that the positions are consistent with PbS, while CuS peaks are absent as indicated in table (1). Furthermore, it is observed that as the CuS content increases, the peak intensity decreases, and the full width at half maximum (FWHM) narrows. This indicates that PbS dominates the compound formation. The reason for this behavior lies in the fact that increased lead ions promote larger crystal formation and reduce crystal defects, leading to a preferred growth orientation for PbS. The stronger ionic bond between sulfur and lead ions compared to that between sulfur and copper ions further supports this dominance, consistent with previous studies [22,23], despite differences in preparation methods.

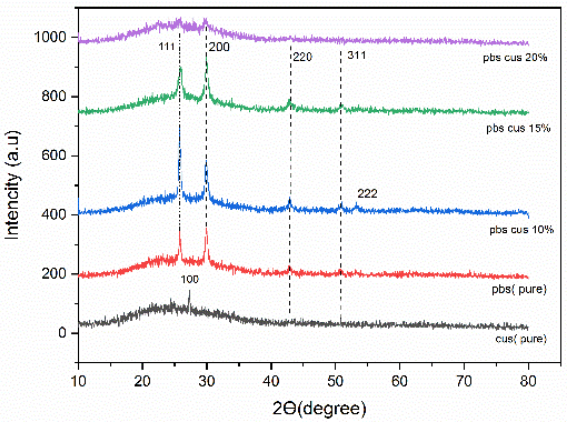

Fig. (2) XRD patterns of the PbS/CuS thin films prepared with different addition ratios of CuS (10%, 15%, 15%)

As shown in Fig. (3), through examination with atomic force microscopy (AFM), it was observed that the prepared film materials were uniformly distributed, with no irregular clusters or voids present on the surfaces of the films. Overall, the images showed consistent vertical height distribution, as detailed in table (2).

In Fig. (4), the topography of the thin film surfaces for all prepared samples was studied using field-emission scanning electron microscope (FE-SEM). The FE-SEM images of PbS/CuS composite films prepared with varying CuS addition ratios (20%, 15%, 10%) reveal that the surfaces of the prepared thin films are nanostructured, consisting of closely packed grains aligned in a highly organized manner. Additionally, the grains are spherical in shape, with notable flower-like structures appearing prominently at the 10% CuS ratio. The grain sizes decrease as the

CuS addition ratio increases. Table (3) summarizes the results, demonstrating a clear decrease in average grain size with increasing film thickness. These observations align with the XRD results, confirming the nanostructured nature of the films. These findings are consistent with the outcomes of the study referenced in [22,24].

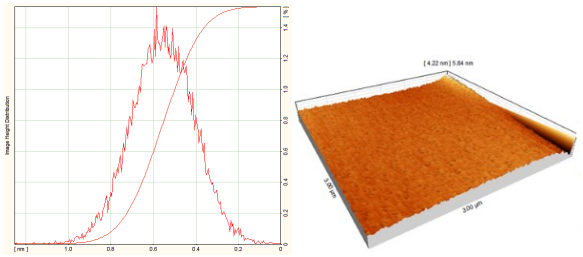

(a) 10%

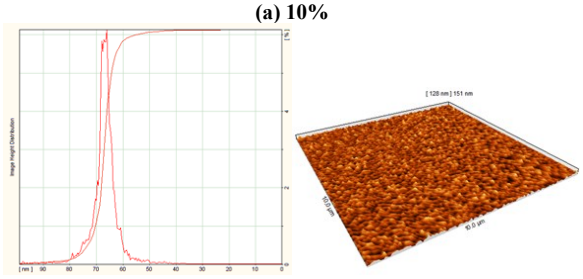

(b) 15%

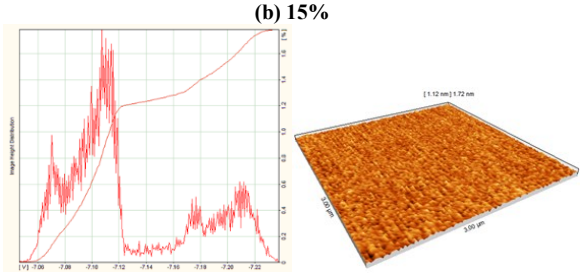

(c) 20%

Fig. (3) AFM results for the PbS/CuS thin films prepared with different CuS addition ratios (20%, 15%, 10%)

Table (2) Values of surface roughness, root mean square (RMS) roughness, and average grain size for the PbS/CuS thin films with varying CuS addition ratios

Sample	Surface Roughness (nm)	RMS (nm)	Average Grain Size (nm)
PbS/CuS 10%	3.77	5.71	54.62
PbS/CuS 15%	1.98	2.94	28.91
PbS/CuS 20%	3.36	4.70	14.8

In Fig. (5), the absorption spectra of the PbS/CuS thin films were measured within the range of 300–1100 nm. The results indicate that the absorbance decreases with an increase in the CuS addition ratio. This reduction in absorbance can be attributed to a decrease in the crystallinity of the films, making the structure more amorphous. Consequently, there is an increase in the scattering of the incident radiation, leading to a reduction in film absorbance. This outcome aligns with previous findings reported in [23] despite differences in preparation methods.

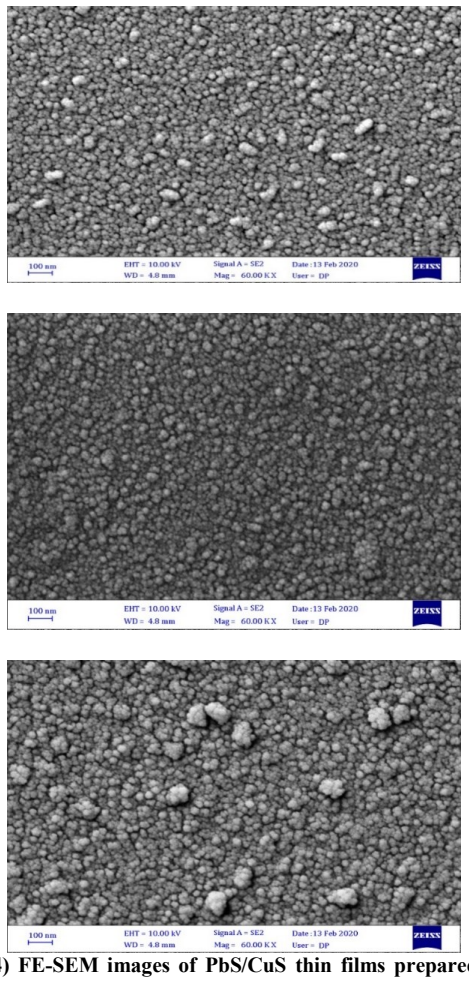

Fig. (4) FE-SEM images of PbS/CuS thin films prepared with different CuS addition ratios

Table (3) Values of the average grain size of PbS/CuS thin films

Sample	Average Grain Size (nm)
PbS/CuS 10%	35.3
PbS/CuS 15%	27.92
PbS/CuS 20%	22.33

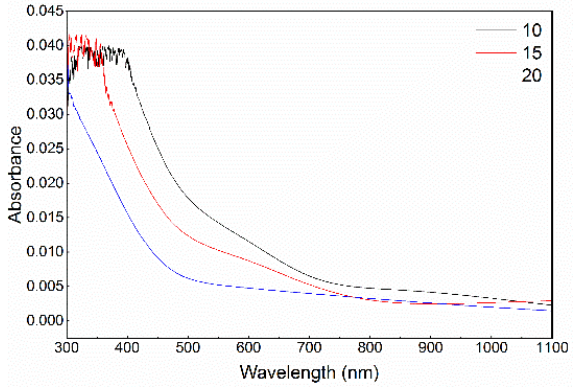

Fig. (5) Absorption spectra of PbS/CuS films prepared with different CuS addition ratios

In Hall measurements were performed for the PbS/CuS composite, which was determined to be of

the (p-type) type, indicating that the majority carriers are holes. This observation aligns with [24]. Using the Hall coefficient (R_H), various electrical parameters were experimentally determined, including the carrier concentration, mobility, conductivity (σ), and resistivity. The results of these measurements are summarized in Showing the calculated Hall effect parameters for the prepared PbS/CuS composite, including carrier concentration p-type , mobility of 1.10×10^{3} $Cm^2/v.s$, average Hall coefficient of 49.9 cm^3/c, conductivity of 2.20×10^{2} 1/cm.Ω and resistivity of 4.54×10^{-3} Ω.cm.

The I-V characteristics of the p-(PbS/CuS)/p-Si and p-(PbS/CuS)/n-Si heterojunctions are shown in figures (6) and (7). These results indicate that the p-p junction exhibits a higher saturation current due to its lower barrier height, which reduces the resistance to charge carrier flow across the barrier between the two layers. This facilitates increased charge transport under forward bias conditions. Moreover, the ideal factor (η) being less than 1 suggests that the charge transport mechanism in this junction is close to ideal behavior, with minimal influence from crystal defects or carrier recombination within the depletion region. Such characteristics make the p-p junction advantageous in applications requiring high conductivity.

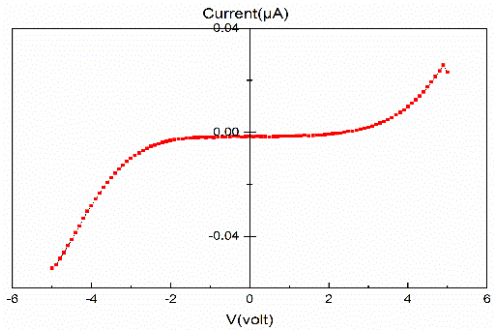

Fig. (6) The current-voltage characteristics of the asymmetric heterojunction (p-(PbS/CuS)/p-Si)

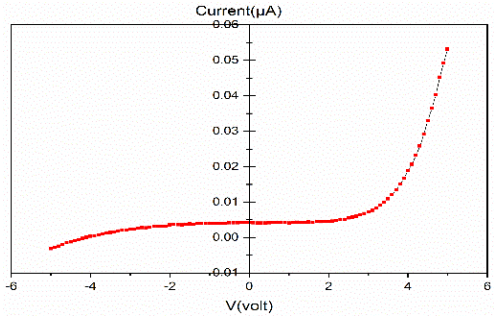

Fig. (7) The current-voltage characteristics of the asymmetric heterojunction (p-(PbS/CuS)/n-Si)

In contrast, the p-n junction demonstrates a lower saturation current due to its higher barrier height, leading to the formation of a wider depletion region between the layers. This reduces the available charge carriers for conduction and results in a lower saturation current. Additionally, the ideal factor being greater than 1 indicates non-ideal electrical behavior, likely due to recombination effects within the barrier region or the presence of crystal defects, which increase resistance and reduce transport efficiency. This behavior can be beneficial in specific applications, such as diodes, where current control is essential, this consistent with the studies [25,26]. By re-plotting the I-V characteristics using logarithmic scaling, as shown in figures (8) and (9), the relationship between log(I)-V for the forward bias current in both heterojunctions can be determined. From this relationship, the saturation current (I_0) can be extracted. The saturation current represents the current flowing through the heterojunction under the condition V = 0.

Using equations (6) and (7), the barrier height (ϕ_B) and the ideality factor (η) of the heterojunctions were calculated as shown in table (4). Figure (6) shows the current-voltage characteristics of the symmetric heterojunction (p (PbS/CuS)/p-Si).

Table (4) Values of I_0, ϕ_B, and η for the symmetric and asymmetric heterojunctions

Heterojunction	Saturation Current (I_0) (μA)	Barrier Height (ϕ_B) (V)	Ideality Factor (η)
p-$(CuS)_x(PbS)_{1-x}$/p-Si	1200	0.247	0.6
p-$(CuS)_x(PbS)_{1-x}$/n-Si	570	0.266	1.2

Capacitance-voltage measurements can be used to study the fundamental properties of semiconductor junctions. In addition to determining the capacitance values of these junctions at specific bias voltages, other information can be derived, such as the built-in voltage (V_{bi}) and information about the carrier concentration and barrier height potential, if data for the prepared thin films are available.

Figure (10) shows the capacitance-voltage characteristics of the symmetric heterojunction (p(PbS/CuS)/p-Si), while figure (11) shows the capacitance-voltage characteristics of the asymmetric heterojunction (p(PbS/CuS)/n-Si). The figures clearly demonstrate how the capacitance of the system changes as a function of the reverse bias voltage within the indicated voltage range. The measurements were performed using aluminum electrodes at a frequency of 1 kHz. It is noted that the capacitance behavior was similar for both cases, and the capacitance value for both cases decreased slightly with increasing reverse bias voltage. This change in capacitance with reverse bias can be attributed to the variation in the accumulated charge at the junction boundaries. The decrease in capacitance for this junction can be linked to the increase in the built-in voltage as the reverse bias voltage increases, which in

turn leads to a widening of the depletion region, this consistent with the studies [27,28].

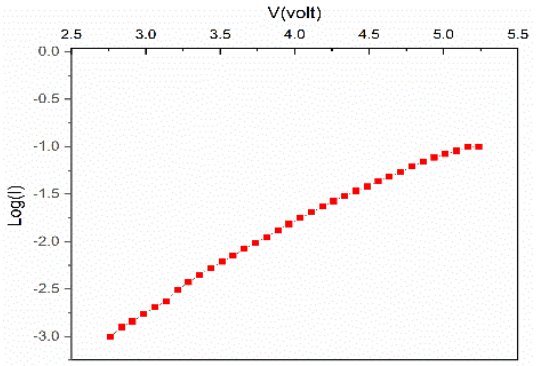

Fig. (8) The relationship between Log I and V for the symmetric heterojunction p(PbS/CuS)/p-Si

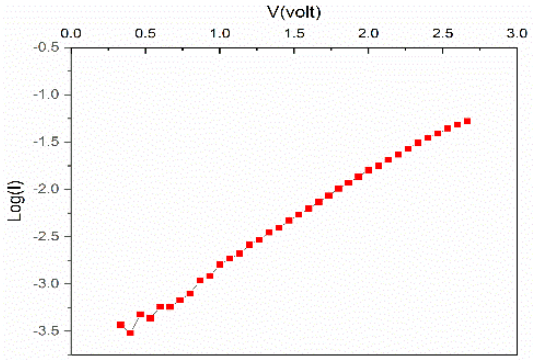

Fig. (9) The relationship between Log(I) and V for the asymmetric heterojunction p(PbS/CuS)/n-Si

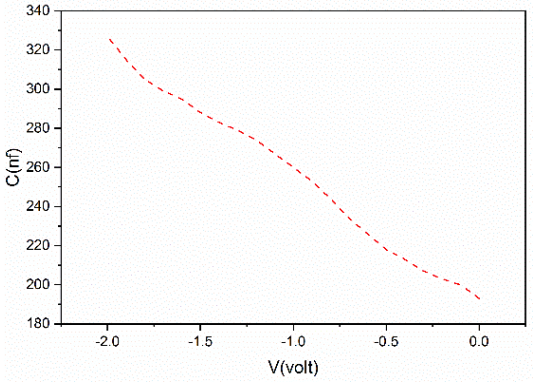

Fig. (10) The capacitance-voltage characteristics of the symmetrical hybrid junction (p(PbS/CuS)/p-Si)

Table (5) Values of capacitance at bias (V=0), built-in potential (V_{bi}), barrier height (ϕ_B), and carrier concentration for the hybrid junction

Heterojunction	C_0 (nF)	V_{bi} (V)	ϕ_B (V)	N_A (m^{-3})
p-$(CuS)_x(PbS)_{1-x}$/p-Si	170	0.2	0.365	$66.17x10^{21}$
p-$(CuS)_x(PbS)_{1-x}$/n-Si	210	0.4	0.090	$1.16x10^{22}$

Figures (12) and (13) show the Mott-Schottky plot, which illustrates the relationship between $1/C^2$ as a function of the applied voltage for both the symmetric heterojunction (p(PbS/CuS)/p-Si) and the asymmetric heterojunction (p(PbS/CuS)/n-Si), respectively. It is observed that these plots represent a straight line, intersecting the x-axis, which represents the bias voltage. The intersection point where $C^{-2}=0$ corresponds to the built-in voltage (V_{bi}). The slope of this straight line represents the carrier concentration of the active layer in the heterojunction.

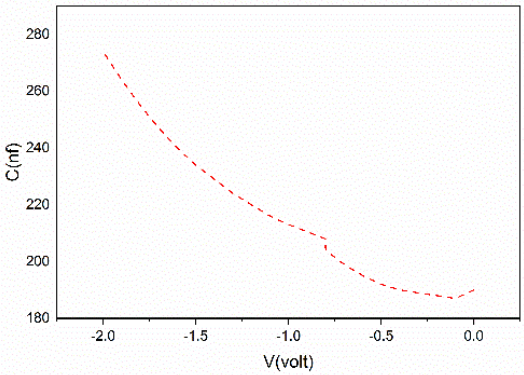

Fig. (11) The capacitance-voltage characteristics of the asymmetrical hybrid junction (p(PbS/CuS)/n-Si)

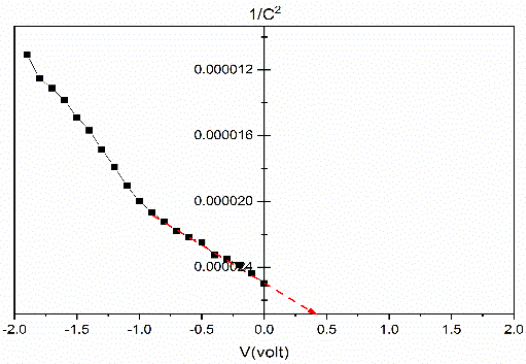

Fig. (12) The relationship between $1/C^2$ and the applied voltage for the symmetrical hybrid junction (p(PbS/CuS)/p-Si)

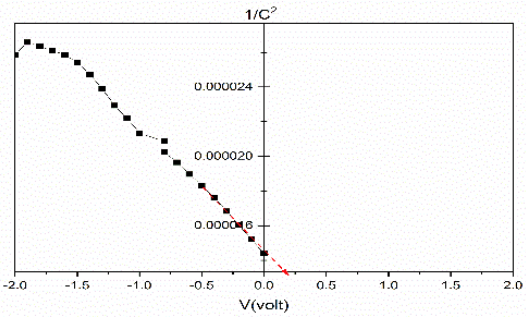

Fig. (13) The relationship between $1/C^2$ and the applied voltage for the asymmetrical hybrid junction (p(PbS/CuS)/n-Si)

4. Conclusions

Based on the results obtained from the study of the structural, optical, and electrical properties of the PbS/CuS composite films, these films were polycrystalline with a cubic structure. They had homogeneous surfaces with nanostructured morphologies without irregular agglomerations or voids. A gradual decrease in absorbance with

increasing addition ratio was indicated due to the reduced crystallinity and the increased optical scattering of the incident radiation, leading to reduced absorption. This suggests that the films become less crystalline as more material is added, affecting their optical properties. These films were p-type their heterojunctions with p- and n-type silicon showed that they were able to rectify current efficiently in both forward and reverse directions.

References

[1] R.C. Agarwal and P.K.C. Pillai, "Chemically Sprayed PbS Coatings for Photothermal Solar Energy Conversion", *J. Appl. Phys.*, 11 (1982) 61-68.

[2] D.S. Albin and S.H. Risbud, "Nucleation and Growth Characteristics of Spray Pyrolyzed CdS Thin Films", *Thin Solid Films*, 147 (1987) 203-212.

[3] J.B. Hagen, "Analytical Expression for the Current-Voltage Characteristics of Organic Bulk Heterojunction Solar Cells", *AIP Adv.*, 10 (2020) 034402.

[4] K.L. Chopra, **"Thin Films Phenomena"**, McGraw-Hill (NY, 1969).

[5] S.M. Sze and K.K. Ng, **"Physics of Semiconductor Devices"**, 3rd ed., Wiley (NY, 2007).

[6] D.A. Neamen, **"Semiconductor Physics and Devices: Basic Principles"**, 4th ed., McGraw-Hill (NY, 2012).

[7] U. Merhan and T. Simanja, "Characterization of Cu_2S-Doped Nanostructured ZnS Thin Films Deposited on Porous Silicon", *Iraqi J. Mater.*, 3(1) (2024) 33-38.

[8] M. Ohring, **"The Materials Science of Thin Films"**, Academic Press (NY, 1992).

[9] G. Hass and R.E. Thin, **"Physics of Thin Films"**, Academic Press (NY, 1988).

[10] Z. Almahmoud, I. Alghoraibi and T. Zaerory, "Morphological Characteristics of Lead Sulfide Thin Films Prepared by Chemical Solution Deposition", *Iraqi J. Mater.*, 1(1) (2022) 15-24.

[11] B.A.M. Bader, O.A. Hamadi and A.K. Yousif, "Measurement of Thermooptic Coefficient in Lead Sulfide Using Laser Single-Beam Scanning Technique", *Eng. Technol. J.*, 25(5) (2007) 683-689.

[12] J.B. Hagen, **"Principles of Microwave Circuits"**, 1st ed., MIT Radiation Laboratory Series, McGraw Hill (NY, 1948).

[13] D.M. Pozar, **"Microwave Engineering"**, 4th ed., John Wiley & Sons (NY, 2011).

[14] A.N. Donald, **"Semiconductors Physics and Devices"**, Irwin (USA, 1992).

[15] S. Ben, **"Solid States Electronic Devices"**, Hall International, Inc. (USA, 1990).

[16] C. Kittel, **"Introduction to Solid State Physics"**, 8th ed., Wiley (NY, 2004).

[17] S.M. Sze, **"Semiconductor Physics and Technology"**, translated by F.G. Hayati and H.A. Ahmed (Mosul, 1990).

[18] M.A. Soliman, A.F. Basha, and S.A. Khairy, **"Solid State Physics"**, Arab Thought Press (2002).

[19] S.M. Ali, "Theoretical Study for the Heterojunction (n-amorphous/p-crystalline Silicon)", M.Sc. thesis, Al-Mustansiriya University, Baghdad (1996).

[20] H.G. Rashid, "Design and Optimization of Thin Films Optical Filters with Application in the Visible and Infrared Region", PhD thesis, Al-Mustansiriya University, Baghdad (1996).

[21] A.A.J., "Preparation and Studying the Physical Properties of SnO_2 Sensor for (NO_2, H_2S, H_2) Gases Detection," MSc thesis, University of Baghdad (2010).

[22] M.K.N.S. Chandran, P.S.K. Nair and R.K. Sharma, "Effect of Copper Sulfide (CuS) Concentration on the Structural, Optical, and Electrical Properties of Thin Films", *J. Mater. Sci. Technol.*, 59 (2022) 242-249.

[23] S.K. Sharma, M.K. Rao and R.N. Gupta, "Effect of Doping on Structural and Morphological Properties of Metal Oxide Nanomaterials", *J. Nanosci. Nanotechnol.*, 22(8) (2022) 4092-4098.

[24] M. Ali and A. Gupta, "Current-Voltage Characteristics and Ideality Factor of Metal-Semiconductor Junctions", *Mater. Sci. Semicond. Process.*, 113 (2020) 104642.

[25] V. Kumar and R. Mehta, "Electrical Characteristics and Ideality Factor of Semiconductor Junctions: A Study of p-n and p-p Junctions", *J. Semicond. Mater. Technol.*, 34(5) (2018) 479-485.

[26] A. Kumar and R. Gupta, "Study of Capacitance-Voltage Characteristics of Metal-Semiconductor and Semiconductor-Semiconductor Junctions", *J. Appl. Phys.*, 124(7) (2018) 075702.

[27] S. Ghosh and R. Mondal, "Capacitance-Voltage and Current-Voltage Characteristics of Asymmetric Junctions", *Mater. Sci. Semicond. Process.*, 109 (2020) 104910.

[28] A.M. Mousa and A.F. Sabbar, "Influence of Post Annealing on the Properties of Cu_XS: Al, Fe Films Deposited by CBD", *Eng. Technol. J.*, 27(14) (2009).

Table (1) Values of inter-planar spacing, peak positions, and Miller indices for the PbS/CuS thin films prepared with different CuS addition ratios (10%, 15%, 20%)

Sample	2θ (Deg.)	d_{hkl} Exp.(Å	d_{hkl} Std.(Å)	FWHM (Deg(.	C.S (nm)	hkl	Phase	card No.
Pure Cus	27.28	3.26	3.28	0.24	34.05	(100)	Hexa gonal	00-0060464
Pure PbS	25.83	3.44	3.42	0.42	19.39	(111)	Cubic	00-005-059
	29.95	2.98	2.96	0.49	16.53	(200)	Cubic	00-0050592
	42.85	2.10	2.09	0.37	22.9	(220)	Cubic	96-9013403
PbS/CuS 10%	25.82	3.44	3.30	0.42	19.26	(111)	Cubic	00-0120174
	29.93	2.98	2.85	0.48	17. 08	(200)	Cubic	00-0120174
	42.87	2.10	2.09	0.38	22.25	(220)	Cubic	00-005-059
	50.50	1.80	1.79	0.22	39.90	(311)	Cubic	00-0050592
	52.86	1.73	1.71	0.24	36.94	(222)	Cubic	00-005-059
PbS/CuS 15%	25.90	3.43	3.30	0.62	13.05	(111)	Cubic	00-0120174
	29.97	2.97	2.85	0.56	14.55	(200)	Cubic	00-012-017
	42.90	2.10	2.96	0.81	10.53	(220)	Cubic	00-005-059
	50.82	1.79	1.79	0.58	15.15	(311)	Cubic	00-0050592
PbS/CuS 20%	29.88	2.98	2.85	0.72	11.41	(200)	Cubic	00-0120174

